Journal of Drug Delivery Science and Technology 81 (2023) 104229

Contents lists available at ScienceDirect

Journal of Drug Delivery Science and Technology

journal homepage: www.elsevier.com/locate/jddst

The evaluation of *in vitro* antichagasic and *anti*-SARS-CoV-2 potential of inclusion complexes of β- and methyl-β-cyclodextrin with naphthoquinone

Verônica da Silva Oliveira [a], Cláudia Cândida Silva [b], Johny Wysllas de Freitas Oliveira [a], Marcelo de Sousa da Silva [a,c], Patricia Garcia Ferreira [d], Fernando de Carvalho da Siva [e], Vitor Francisco Ferreira [d], Euzébio Guimarães Barbosa [a], Cecília Gomes Barbosa [f], Carolina Borsoi Moraes [f,g], Lucio Holanda Gondim de Freitas-Junior [f], Attilio Converti [h], Ádley Antonini Neves de Lima [a,*]

[a] Department of Pharmacy, Health Sciences Center, Federal University of Rio Grande do Norte, Natal, Rio Grande do Norte, 59012-570, Brazil
[b] School of Technology, State University of Amazonas, Manaus, Amazonas, 69065-020, Brazil
[c] Global Health and Tropical Medicine, Institute of Hygiene and Tropical Medicine, NOVA University Lisbon, Lisbon, 1800-166, Portugal
[d] Department of Pharmaceutical Technology, Faculty of Pharmacy, Fluminense Federal University, Niterói, Rio de Janeiro, 24241-002, Brazil
[e] Institute of Chemistry, Fluminense Federal University, Niterói, Rio de Janeiro, 24020-150, Brazil
[f] Department of Microbiology, Institute of Biomedical Sciences, University of Sao Paulo, São Paulo, São Paulo, 05508-900, Brazil
[g] Department of Pharmaceutical Sciences, Federal University of São Paulo, São Paulo, São Paulo, 09913-030, Brazil
[h] Department of Civil, Chemical and Environmental Engineering, University of Genoa, Pole of Chemical Engineering, via Opera Pia 15, 16145, Genoa, Italy

ARTICLE INFO

Keywords:
Inclusion complexes
Naphthoquinone
Anti-SARS-CoV-2
Antichagasic activity

ABSTRACT

The compound 3*a*,10*b*-dihydro-1*H*-cyclopenta[*b*]naphtho[2,3-*d*]furan-5,10-dione (IVS320) is a naphthoquinone with antifungal and antichagasic potential, which however has low aqueous solubility. To increase bioavailability, inclusion complexes with β-cyclodextrin (βCD) and methyl-β-cyclodextrin (MβCD) were prepared by physical mixture (PM), kneading (KN) and rotary evaporation (RE), and their *in vitro anti*-SARS-CoV-2 and antichagasic potential was assessed. The formation of inclusion complexes led to a change in the physicochemical characteristics compared to IVS320 alone as well as a decrease in crystallinity degree that reached 74.44% for the IVS320-MβCD one prepared by RE. The IVS320 and IVS320-MβCD/RE system exhibited *anti*-SARS-CoV-2 activity, showing half maximal effective concentrations (EC_{50}) of 0.47 and 1.22 μg/mL, respectively. Molecular docking simulation suggested IVS320 ability to interact with the SARS-CoV-2 viral protein. Finally, the highest antichagasic activity, expressed as percentage of *Tripanosoma cruzi* growth inhibition, was observed with IVS320-βCD/KN (70%) and IVS320-MβCD/PM (72%), while IVS320 alone exhibited only approximately 48% inhibition at the highest concentration (100 μg/mL).

1. Introduction

COVID-19, caused by the SARS-CoV-2 virus, has spread rapidly on a global scale with a high mortality rate [1]. Despite accelerated scientific progress, even with vaccine development and implementation of vaccination schedule worldwide [2], there is still a lack of treatment options for this disease. So, the search for therapeutic alternatives and development of new drugs against COVID-19 are still necessary. In this sense, drug repositioning is an interesting strategy.

In this context, naphthoquinones, belonging to the quinone class, have a characteristic naphthalene ring, which gives them redox properties that can interfere with oxidative processes in biological systems [3,4]. They have stood out due to biological properties such as anti-inflammatory [5,6], antineoplastic [7–9], antimicrobial [3,10], antifungal [11,12], antiviral [13] and antiparasitic [4,10,14–16] ones.

The naphthoquinone class includes the compound 3*a*,10*b*-dihydro-

* Corresponding author.
E-mail addresses: veronicasoliver47@gmail.com (V.S. Oliveira), claudiacsbr@gmail.com (C.C. Silva), johnywysllas@gmail.com (J.W. de Freitas Oliveira), mssilva.ufrn@gmail.com (M.S. da Silva), patricia.pharma@yahoo.com.br (P.G. Ferreira), fcsilva@id.uff.br (F.C. da Siva), vitorferreira@id.uff.br (V.F. Ferreira), euzebiogb@gmail.com (E.G. Barbosa), cecigomes.barbosa@gmail.com (C.G. Barbosa), cbmoraes@unifesp.br (C.B. Moraes), luciofreitasjunior@gmail.com (L.H.G. Freitas-Junior), converti@unige.it (A. Converti), adley.lima@ufrn.br (Á.A.N. Lima).

https://doi.org/10.1016/j.jddst.2023.104229
Received 21 September 2022; Received in revised form 19 January 2023; Accepted 1 February 2023
Available online 8 February 2023

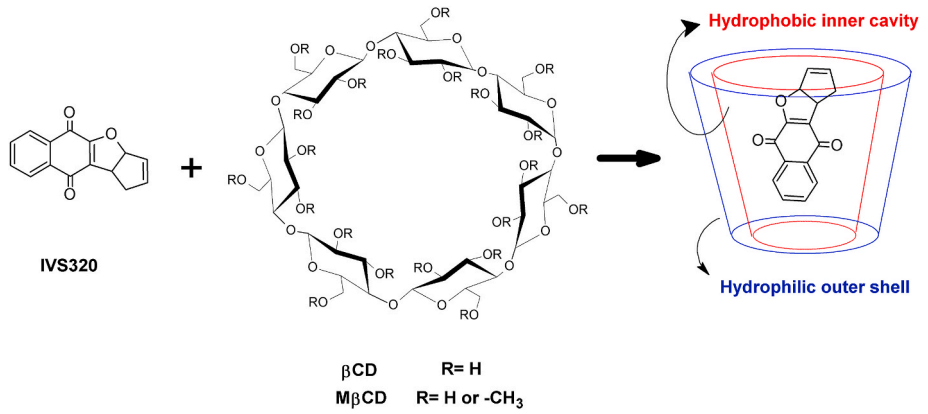

Fig. 1. Scheme of formation of inclusion complexes made up of IVS320 and β-cyclodextrins (βCD) or methyl-β-cyclodextrin (MβCD).

1*H*-cyclopenta[*b*]naphtho[2,3-*d*]furan-5,10-dione (IVS320) (Fig. 1), which has antifungal [17] and antichagasic [18] potential. However, despite its biological potential, it has low water solubility, which results in poor bioavailability.

Since about 30–70% of new drug candidates have low solubility in aqueous medium [19], pharmacokinetic optimization studies are part of their development protocol. Several methods can be used to increase the solubility and dissolution rate of lipophilic compounds, among which are obtaining solid amorphous forms, nanoparticles, salty formulations [20] and solid dispersions [20,21 as well as developing water-soluble inclusion complexes [22,23].

The formation of inclusion complexes with cyclodextrins (CDs) is one of the most used ways to increase drug solubility [24]. CDs can interact with organic molecules through intermolecular bonds forming so-called inclusion complexes, which normally have greater solubility, bioavailability and chemical stability [25] and exhibit activity both *in vitro* and *in vivo* [26].

CDs, which are composed of D-glucopyranose units linked together to form cyclic conical structures, can have natural or synthetic origin. They are characterized by a trunk-conical shape with a hydrophilic outer face that allows interaction in a polar environment and a highly hydrophobic cavity able to include poorly soluble drugs [27]. Among natural CDs, β-cyclodextrin (βCD), made up of 7 glucose units [22,28], is widely used because its internal cavity has a size suitable for inclusion of compounds. Despite being obtained with high degree of purity, good yield and low cost, it has low solubility [29].

To increase their solubility, CDs have been modified by the addition of methyl, hydroxyalkyl, ester or ether groups [23,25]. Particularly, methyl-β-cyclodextrin (MβCD) is a βCD derivative obtained by methylation that has higher solubility in water and less toxicity than natural βCD [30].

Looking for new chemical entities and given the biorelevant properties of naphthoquinones, the present work aimed to develop new inclusion complexes of IVS320 with βCD and MβCD in order to a) evaluate their antichagasic activity, b) obtain new drugs with less toxicity and greater efficacy than benznidazole as a reference drug, and c) assess their *anti*-SARS-CoV-2 activity in *in vitro* antiviral screening assays.

2. Materials and methods

2.1. Materials

The compound 3*a*,10*b*-dihydro-1*H*-cyclopenta[*b*]naphtho[2,3-*d*]furan-5,10-dione (IVS320) was synthesized by the Laboratory of Applied Organic Synthesis (LabSOA) at the Fluminense Federal University following the methodology reported by Ref. [17]. β-cyclodextrin (βCD) (MW = 1134.98 g/mol; Cod. C4805) and methyl-β-cyclodextrin (MβCD) (Mw ~1320 g/mol; Cod. C4555) were purchased from Sigma-Aldrich (St. Louis MO, USA). All solvents used were of analytical grade.

2.2. Synthesis of the inclusion complexes

The inclusion complexes were prepared by three methods, namely physical mixture (PM), kneading (KN) and rotary evaporation (RE), using a 1:1 (w/w) IVS320:cyclodextrin molar ratio.

To prepare inclusion complexes by PM, each of the cyclodextrins was weighed and mixed with IVS320 using a mortar and pestle, and the resulting solid was stored in a desiccator. As for KN, IVS320 and the selected cyclodextrin was weighed and homogenized, and then a 50:50 (v/v) water/acetone solution was added as a solvent. The samples were dried in an oven for 8 h at 50 °C, and the solid was stored in a desiccator. As for RE, βCD or MβCD was solubilized in the same 50:50 (v/v) water/acetone solution, and then IVS320 was added. The solution was magnetically stirred for 72 h at 25 °C. The solvent was then removed with a rotary evaporator (IKA RV10, GEHAKA, Staufen, Germany) at 50 °C, and the solid was stored in a desiccator.

2.3. Characterization of inclusion complexes

2.3.1. Thermal analysis

Differential scanning calorimetry (DSC) was performed in the temperature range of 25–500 °C with a DSC-50 calorimeter (Shimadzu, Tokyo, Japan) at a heating rate of 10 °C.min^{-1}, under dynamic atmosphere of N_2 (50 mL min^{-1}), using an alumina crucible containing a sample mass of around 4 mg. Before the test, the equipment was calibrated using a standard of indium and zinc.

Thermogravimetry (TG) was performed on a DTG-60 thermogravimetric analyzer (Shimadzu, Tokyo, Japan) in the temperature range of 30–900 °C under the same conditions, using about 3 mg of sample. The empty alumina crucible served as a reference. Instrument calibration was performed with an aluminum and zinc standard.

2.3.2. Fourier Transform Infrared Spectroscopy

Fourier Transform Infrared Spectroscopy (FTIR) analyses were conducted using an IRPrestige-21 spectrometer (Shimadzu, Kyoto, Japan) equipped with the selenium crystal accessory. The samples were subjected to reading in the 4000 to 600 cm^{-1} region, with 15 scans and 4 cm^{-1} resolution.

2.3.3. X-ray diffraction

The X-ray Diffraction (XRD) analysis was performed using a XRD 6000 X-ray diffractometer (Shimadzu) operated at 40 kV, 30 mA, at a speed of 2°.min^{-1}, with a scan from 2 to 80°.

The degree of crystallinity (x) of samples was calculated using the Shimadzu software [31] by the equation:

$$x = \frac{1}{1 + K \times \frac{I_a}{I_{cr}}} \quad (1)$$

where I_{cr} is the integrated intensity of the crystalline part, I_a is that of the amorphous fraction, and K is the ratio between the X-ray scattering intensity of the amorphous fraction of a converted mass and that of the crystalline fraction.

2.3.4. Scanning Electron Microscopy

Scanning Electron Microscopy (SEM) was carried out using a TM-3000 Tabletop Microscope (Hitachi, Tokyo, Japan). Samples were fixed using a double layer carbon tape, and micrographs taken at an excitation voltage of 15 kV and a magnification factor of 1500 × .

2.4. Antiviral screening against SARS-CoV-2

2.4.1. Systems

The antiviral activity of IVS320 and IVS320-βMCD/RE systems was assessed, the latter having been selected due to the significant crystallinity reduction observed (see section 3.1.4). After dissolution in dimethyl sulfoxide (DMSO) (Sigma-Aldrich) up to a concentration of 2 mg/mL, each system was 33.33-fold diluted in Phosphate Buffered Saline (PBS), and 10 μL of each sample were transferred to the assay plates, thus obtaining a final dilution factor of 200. Either compound was tested in dose response mode at an initial concentration of 10 μg/mL.

2.4.2. Virus strain

A nasopharyngeal sample from a patient diagnosed with COVID-19 in the Hospital Israelita Albert Einstein, São Paulo, Brazil, was used to isolate the SARS-CoV-2 virus (HIAE-02: SARS-CoV2/SP02/human/2020/BRA, GenBank Accession No. MT126808.1). All procedures involving the virus were performed in the level 3 biosafety laboratory of the Institute of Biomedical Sciences of the São Paulo University.

2.4.3. Cell lines and viral infection

Vero cells (CCL-81) were infected with low passage SARS-CoV-2 maintained in DMEM-High Glucose (Sigma-Aldrich, St. Louis, MO, USA) supplemented with 2% heat-inactivated Fetal Bovine Serum (FBS) (Thermo Fisher Scientific, Waltham, MA, USA), 100 U/mL of penicillin and 100 μg/mL of streptomycin (Thermo Fisher Scientific, Waltham, MA, USA). Cells were then maintained at 37 °C in a humidified atmosphere at 5% CO_2. Aliquots of the supernatant of the infected cell culture were collected after 48–72 h post-infection and stored at −80 °C. The viral titer was determined by plaque assay in Vero CCL-81 as described by Ref. [32].

2.4.4. Phenotypic assay with SARS-CoV-2

Vero cells were seeded in 384-well plates in DMEM-High Glucose. After 24 h, the cells received the systems, and then SARS-CoV-2 viral particles were added at 0.1 multiplicity of infection. After 36 h, plates were fixed in 4% paraformaldehyde in PBS (pH 7.4), immunofluorescence was performed with serum from COVID-19 patients, and images were acquired and analyzed by the Operetta High Content Imaging System (PerkinElmer, Waltham, MA, USA). Chloroquine diphosphate was added as the viral infection inhibition control.

2.4.5. Data analysis

The total numbers of cells and infected cells were measured in each of the wells using the High Content Analysis software (Harmony, PerkinElmer, Waltham, MA, USA). The reduction in the number of infected cells was taken as an index of antiviral activity of samples and expressed as a percentage of controls. From the infected and uninfected controls, the activity of each system was normalized. Concentration-response curves plotted using normalized activity were used to calculate, by the GraphPad Prism Software version 5.0 (GraphPad Software Inc., La Jolla, CA, USA), the half maximal effective concentration (EC_{50}) of each system, i.e., the concentration able to reduce the infection by 50% compared to untreated infected controls.

2.5. 3CL protease molecular docking simulations

All possible four IVS320 stereoisomers (*RR*, *RS*, *SS*, and *SR*) were built using the Avogadro software [33]. The created structures were geometry optimized using the Molecular Orbital Package (MOPAC) software according to the semiempirical method PM7 [34]. The UCSF chimera software [35] was used to process one binding site of 3CL protease from SARS-CoV-2 (PDB Id: 6M2N) [36]. The ligand was removed from the binding site, and IVS320 molecular models of all configurations were docked. The Autodock Vina software [37] was used to produce binding poses as well as ligand-$3CL^{pro}$ affinities. The complex $3CL^{pro}$-IVS320 was geometry optimized using molecular mechanics implement in the USCF Chimera's Minime Structure application. The molecular docking poses were used to interpret IVS320 *anti*-SARS-CoV-2 activities.

2.6. Antichagasic activity

2.6.1. Parasite

To obtain the epimastigote form, the Y strain of *Tripanosoma cruzi* was grown in Liver Infusion Tryptose (LIT) medium supplemented with 10% FBS and 5% 100 UI/mL penicillin (antibiotic against streptococci) at 27 °C in a Biochemical Oxygen Demand (BOD) oven.

2.6.2. In vitro antichagasic activity

The *in vitro* antichagasic activity assays were conducted using the epimastigote form of *T. cruzi* at a concentration of 1×10^7 parasites/mL. Briefly, stock solutions of IVS320, IVS320-βCD and IVS320-MβCD were prepared using DMSO as the solvent. Subsequently, the stock solutions were diluted in culture medium in 96-well plates to obtain concentrations of the systems in the range of 100 to 2.5 μg/mL. Then, the epimastigote form of *T. cruzi* was applied in each well, and the plates were incubated for 24 h. Positive control (medium and strain), negative control (medium and compound) and solvent control (DMSO, medium and strain) were used in the assays. In addition, benznidazole was used as a trypanocidal reference drug.

The inhibition of parasite growth was assessed by the resazurin reduction assay (Sigma-Aldrich). After 24 h of incubation, the absorbance was read at 570 and 600 nm in the microplate reader (Epoch, BioTek Instruments, Winooski, VT, USA). All experiments were performed in triplicate, and the inhibition percentage was calculated using the following formula:

$$\%\ \text{Inhibition} = 100 - \left(\left(A\_(570t) - \left(A\_(600t) \times R_0\right)\right) / \left(A_{570c} - \left(A_{600c} \times R_0\right)\right)\right) \times 100 \quad (2)$$

where A_{570t} and A_{600t} are the absorbances of the treatment at 570 and 600 nm, A_{570c} and A_{600c} are the absorbances of the positive control at 570 and 600 nm, while

$$R_0 = A_{570m}/A_{600m} \quad (3)$$

is a correction factor taking into account the medium interference with

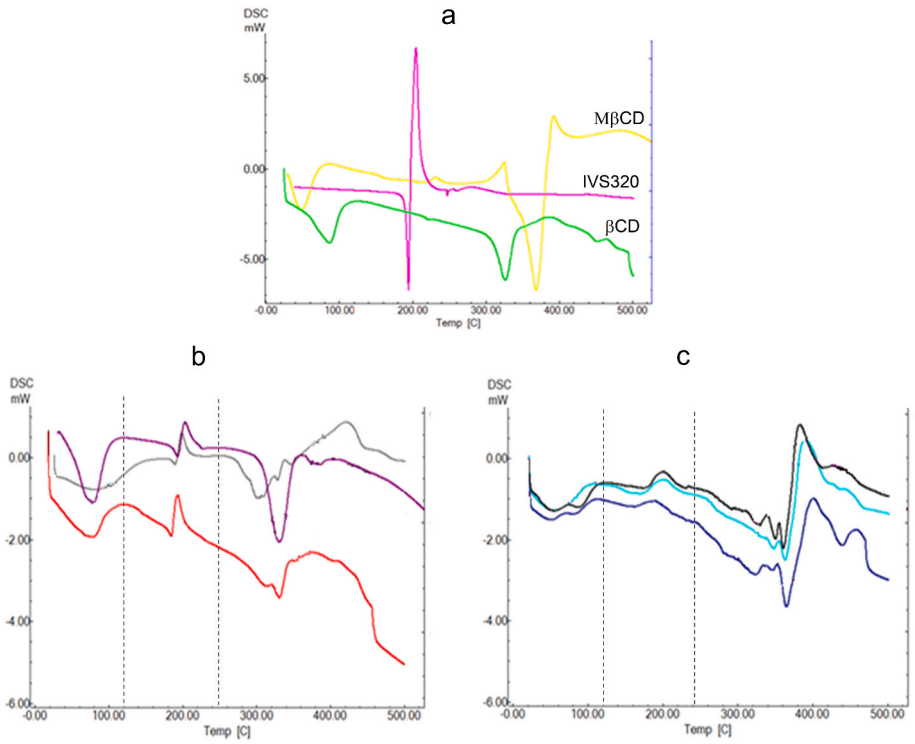

Fig. 2. DSC curves in nitrogen atmosphere (50 mL min^{-1}) of (a) single compounds: IVS320 (pink), βCD (green), MβCD (yellow); (b) IVS320-βCD systems prepared by physical mixture (purple), kneading (gray), rotary evaporation (red); (c) IVS320-MβCD systems prepared by physical mixture (black) kneading (light blue), rotary evaporation (dark blue). (For interpretation of the references to colour in this figure legend, the reader is referred to the Web version of this article.)

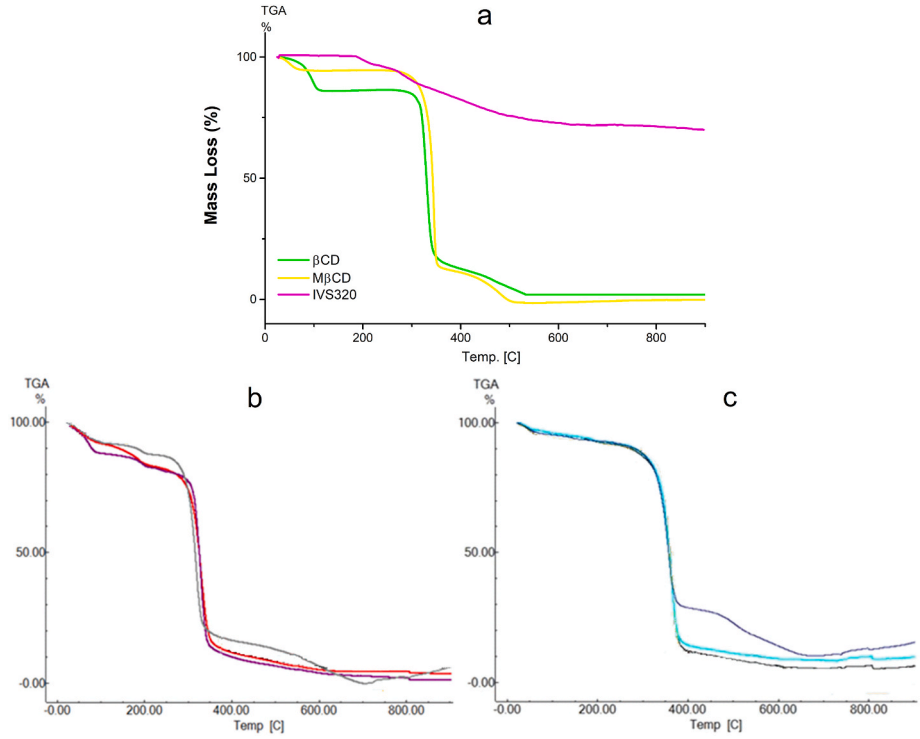

Fig. 3. TG curves in nitrogen atmosphere (50 mL min^{-1}) of (a) single compounds: IVS320 (pink), βCD (green), MβCD (yellow); (b) IVS320-βCD systems prepared by physical mixture (purple), kneading (gray), rotary evaporation (red); (c) IVS320-MβCD systems prepared by physical mixture (black), kneading (light blue), rotary evaporation (dark blue). (For interpretation of the references to colour in this figure legend, the reader is referred to the Web version of this article.)

resazurin, being A_{570m} and A_{600m} the absorbances of the medium at 570 and 600 nm, respectively.

2.6.3. Statistical analysis

The data obtained were evaluated through the one-way analysis of variance (ANOVA) followed by the Dunnett's *t*-test for multiple comparisons. Values were expressed as mean ± standard error of the mean. Values of $p < 0.05$ were considered statistically significant. Statistical analyses were performed using the GraphPad Prism Software version 5.0 (GraphPad Software Inc.).

3. Results and discussion

3.1. Characterization of inclusion complexes

3.1.1. Differential scanning calorimetry

Thermal analysis techniques were used to evaluate the thermal behavior of the individual components and the inclusion complexes as well as possible changes ascribable to their formation.

The Differential Scanning Calorimetry (DSC) curve of IVS320 (Fig. 2a) revealed two events. The first endothermic event, occurred between 185 and 194 °C, is characteristic of fusion (T_{peak} 189 °C, ΔH 260 J g^{-1}), while the second exothermic event, took place between 194 and 218 °C (T_{peak} 203 °C, ΔH 297 J g^{-1}), was the likely result of recrystallization, indicating a change to another crystalline form [18].

On the other hand, the DSC curve of β-cyclodextrin (βCD) showed a first endothermic event between 49 and 118 °C (T_{peak} 86 °C, ΔH 176 J g^{-1}) ascribable to water loss [27] and a second endothermic event between 298 and 360 °C (T_{peak} 326 °C, ΔH 155 J g^{-1}) likely due to βCD decomposition [22].

The thermogram of IVS320-βCD system prepared by physical mixture (PM) showed an endothermic peak at 192 °C and an exothermic one at 203 °C, corresponding to IVS320 fusion and recrystallization, respectively. An additional endothermic event occurred at 330 °C resembles the decomposition profile of βCD alone.

The same fusion and recrystallization events took place at 189 and 198 °C in the IVS320-βCD system prepared by kneading (KN) and at 186 and 194 °C in the one prepared by rotary evaporation (RE). Such a persistence of IVS320 fusion events indicates the drug microcrystalline form in the systems. Both systems showed additional events in the 250–350 °C range (Fig. 2b) corresponding to βCD degradation, which suggests different decomposition steps resulting from IVS320 and βCD interaction.

Shifts in melting and recrystallization events were observed for the βCD-containing systems compared to IVS320, and, among them, the IVS320-βCD/KN and IVS320-βCD/RE ones also showed a significant decrease in the heat flow, thus suggesting the formation of inclusion complexes. According to Ref. [38]; when the host molecules are stabilized in the cyclodextrin cavity, usually their melting, boiling or sublimation peaks are shifted to a different temperature or even disappear.

Regarding the DSC curve of methyl-β-cyclodextrin (MβCD), two endothermic events were observed, the first in the range 40–100 °C due to water loss [39,40] and the second at about 392 °C due to decomposition.

The thermograms of IVS320-MβCD systems showed two endothermic events below 100 °C (Fig. 2c), which may be the result of water release from the outer and inner part of MβCD, while the endothermic peak related to IVS320 fusion was not clearly detected by DSC, suggesting that the formation of complexes gave the drug an amorphous state. The exothermic event was shifted to lower temperatures compared to IVS320, i.e., 200, 195 and 190 °C for IVS320-MβCD/PM, IVS320-MβCD/KN and IVS320-MβCD/RE, respectively, likely due to the interaction between drug and MβCD. Additionally, while MβCD exhibited only one endothermic event, with a well-defined peak ascribable to its degradation, several endothermic events were observed for IVS320-MβCD systems from 318 to 400 °C, which can be assigned to different

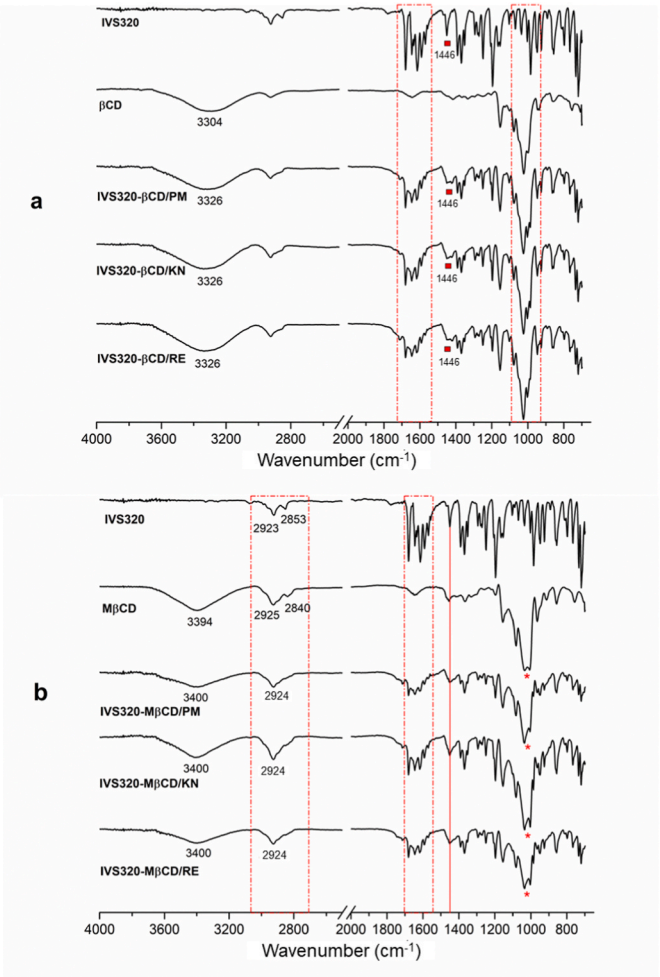

Fig. 4. FTIR Spectra of (a) IVS320, βCD, and their inclusion complexes prepared by physical mixture (IVS320-βCD/PM), kneading (IVS320-βCD/KN), rotary evaporation (IVS320-βCD/RE); (b) IVS320, MβCD, and their inclusion complexes prepared by physical mixture (IVS320-MβCD/PM), kneading (IVS320-MβCD/KN), rotary evaporation (IVS320-MβCD/RE).

stages of MβCD degradation induced by the formation of inclusion complexes.

These results taken as a whole demonstrate that changes in IVS320 thermal profile were much more evident in systems prepared with MβCD than with βCD, and among these the IVS320-MβCD/KN and IVS320-MβCD/RE complexes showed the strongest interaction between IVS320 and MβCD.

3.1.2. Thermogravimetric analysis

The thermogravimetric (TG) curve of IVS320 (Fig. 3a) evidenced a first event in the temperature range of 160–262 °C with a mass loss of 5%, a second mass loss of 6.25% (T_{onset} 262 °C, T_{endset} 315 °C) due to the beginning of its decomposition, and a third event between 315 and 900 °C with a mass loss of 18.73%. The high thermal resistance of IVS320 is consistent with the characteristics of some compounds belonging to the naphthoquinone class [41].

In the TG curve of βCD it can be observed a mass loss of 12.25% due to dehydration (T_{onset} 49 °C, T_{endset} 97 °C) followed by a second event responsible for a mass loss of 70.80% (T_{onset} 310 °C, T_{endset} 360 °C) related to βCD decomposition, thus confirming literature data [26].

It was possible to observe a significant reduction in water loss in the TG profiles of complexes made up of IVS320 and βCD compared to βCD alone (Fig. 3b). In fact, the IVS320-βCD/PM, IVS320-βCD/KN and IVS320-βCD/RE systems showed mass losses due to dehydration of only

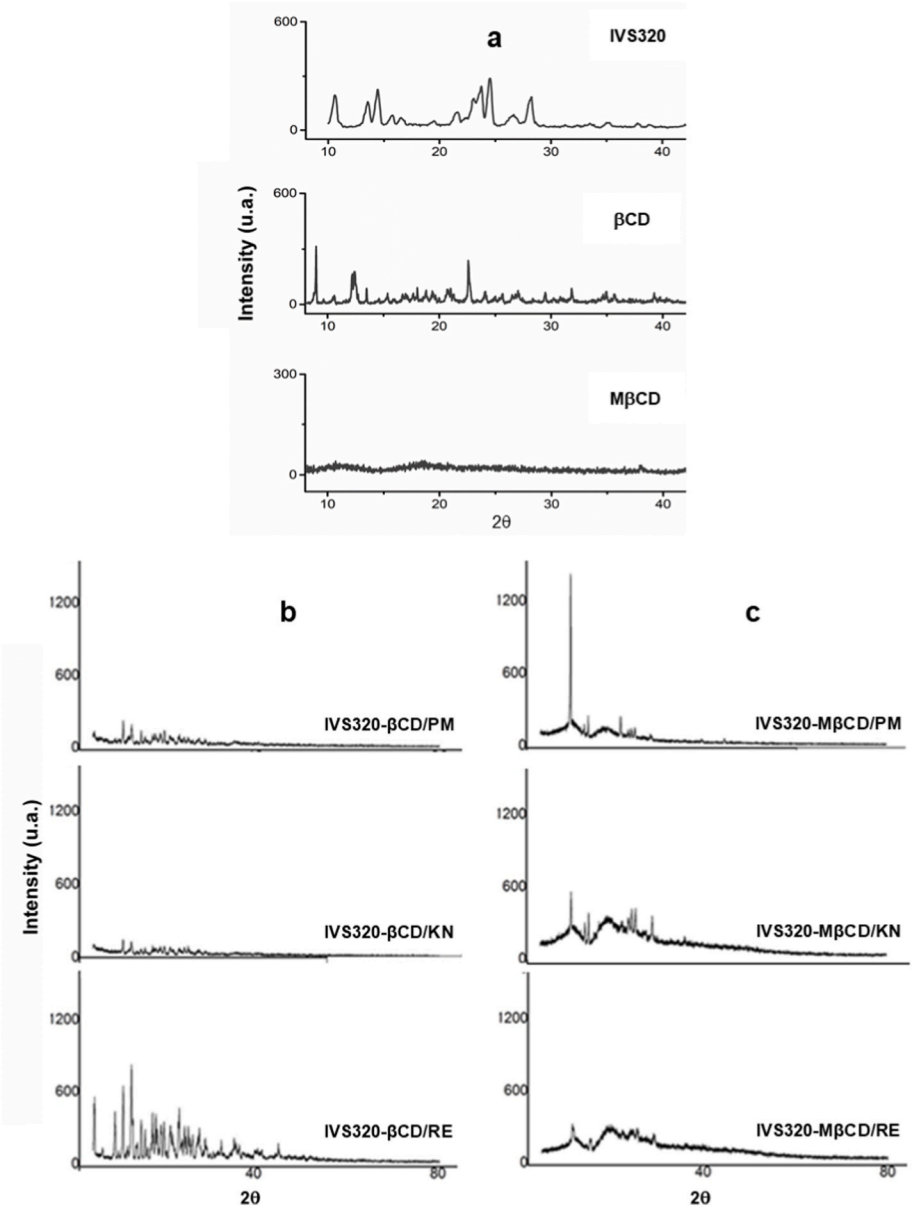

Fig. 5. XRD of (a) single compounds: IVS320, βCD, MβCD; (b) IVS320-βCD systems prepared by physical mixture (IVS320-βCD/PM), kneading (IVS320-βCD/KN), rotary evaporation (IVS320-βCD/RE); (c) IVS320-MβCD systems prepared by physical mixture (IVS320-MβCD/PM), kneading (IVS320-MβCD/KN), rotary evaporation (IVS320-MβCD/RE).

9.70% (T_{onset} 30 °C, T_{endset} 85 °C), 6.84% (T_{onset} 29 °C, T_{endset} 97 °C) and 6.22% (T_{onset} 33 °C, T_{endset} 84 °C), respectively. Such a behavior can be attributed to the decrease in the water amount in the complexes cavity due to the presence of the drug and its interaction with βCD [42].

In turn, the most significant event in the thermograms of the IVS320-βCD systems can be attributed to their thermal degradation occurred in the temperature range of 256–368 °C, which was responsible for mass losses of approximately 64–68%, with almost negligible influence of the preparation method.

The MβCD thermogram (Fig. 3a) revealed a dehydration event started at 31 °C and extended to 73 °C, with a mass loss of 3.55% [43], followed by a second event in the range of 322–391 °C, with a mass loss of 83.37%, which can be ascribed to MβCD thermal decomposition [44].

Contrary to the IVS320-βCD systems, drug incorporation into MβCD did not appear to influence the first event compared to MβCD alone, leading to mass losses of 1.80% (T_{onset} 30 °C, T_{endset} 52 °C), 2.52% (T_{onset} 30 °C, T_{endset} 62 °C) and 3.52% (T_{onset} 30 °C, T_{endset} 64 °C) using PM, KN and RE, respectively. On the other hand, it reduced the mass loss of the second one to only 74.39% (T_{onset} 295 °C, T_{endset} 387 °C), 74.50% (T_{onset} 295 °C, T_{endset} 387 °C) and 58.73% (T_{onset} 291 °C, T_{endset} 379 °C), respectively. This result suggests some thermal stabilization of MβCD structure induced by drug interaction, especially in the case of the system prepared by RE.

3.1.3. Fourier Transform Infrared Spectroscopy

The Fourier Transform Infrared Spectroscopy (FTIR) spectrum of IVS320 (Fig. 4) showed bands at 1678 and 1644 cm^{-1} corresponding to C=O asymmetric and symmetric stretching, while vibrational modes related to the stretching of C=C of the naphthoquinone and cyclopentene ring were found at 1614, 1591 and 1568 cm^{-1}. Additionally, the vibrational modes with strong intensity observed at 1194 cm^{-1} (ν(C–O–C)) and with moderate intensity observed at 1157 and 1035 cm^{-1} are characteristic of the ν(C–O) of cyclic ethers.

βCD showed a broad and intense band at 3304 cm^{-1}, corresponding to the hydroxyl group stretching, while the C–H stretching was found at 2927 cm^{-1}. The additional bands observed at 1152, 1076 and 1023

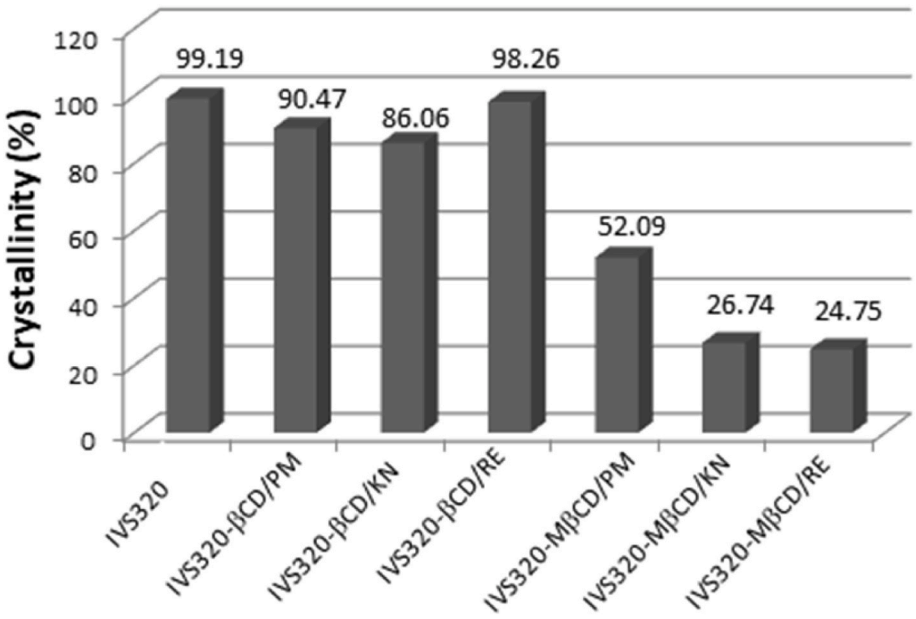

Fig. 6. Crystallinity degree of IVS320, IVS320-βCD systems and IVS320-MβCD systems obtained by physical mixture (PM), kneading (KN) and rotary evaporation (RE).

cm^{-1} can be assigned to the stretching of C–O of the ether and hydroxyl groups. In turn, MβCD exhibited band at 3394 cm^{-1} referring to ν(O–H) and vibrational modes at 2925 and 2840 cm^{-1} corresponding to stretching of C–H. Bands were found at 1152, 1080 and 1036 cm^{-1} corresponding to the C–O stretching of ether and hydroxyl groups, similar to literature [38].

Spectra of IVS320-βCD systems prepared by the three methods (Fig. 4a) showed vibrational modes confirming the presence of βCD, through the appearance of O–H stretching, which was displaced from 3304 cm^{-1} (βCD alone) to 3326 cm^{-1}. In IVS320-MβCD systems (Fig. 4b), MβCD O–H stretching was displaced from 3394 to 3400 cm^{-1}, while the two vibrational modes relating to asymmetrical and symmetrical C–H stretching were no longer clearly evident in the 3000-2800 cm^{-1} range compared to IVS320 and MβCD, being found at 2924 cm^{-1} for all methods.

Additionally, for both systems (IVS320-βCD and IVS320-MβCD) obtained by the three methods, in the range of 1680 to 1590 cm^{-1} there were changes in the profile of bands referring to C=O and C=C stretching, compared to IVS320 alone. Modifications were also observed in the band profile between 1023 and 1036 cm^{-1}, referring to IVS320-βCD and IVS320-MβCD systems, respectively, compared to the C–O deformation of cyclodextrins alone.

Considering the chemical structures of IVS320 and cyclodextrins employed (βCD and MβCD), as well as the changes observed in the spectra of systems obtained by the three methods, it is possible to propose the formation of inclusion complexes by formation of intermolecular hydrogen bridges between cyclodextrin hydroxyl groups and carbonyl groups and/or oxygen atoms (cyclic ether) of IVS320.

Despite the use of distinct methods to obtain systems, the results of FTIR did not show significant changes among them. The most relevant changes were due to the use of different cyclodextrins rather than to different preparation methods.

3.1.4. X-ray diffraction

The crystallinity of compounds was investigated by X-ray Diffraction (XRD), whose results are illustrated in Fig. 5. The IVS320 diffractogram revealed high intensity crystalline reflections at 10.50°, 14.34°, 24.38° and 28.22°, followed by secondary reflections. This result was confirmed by the very high IVS320 crystallinity degree (99.19%) (Fig. 6) calculated following the approach of [40].

βCD exhibited crystalline characteristics as well, with intense reflections at 4.40°, 8.90°, 12.30° and 22.60° [22,27], whereas the MβCD diffraction pattern revealed two wide halos at around 11.0° and 18.0°, indicating its amorphous nature [39,40].

The diffractograms of the IVS320-βCD/PM and IVS320-βCD/RE systems (Fig. 5b) showed only very small variations compared to that of pure IVS320, practically overlapping it, which is consistent with the quite high retention (90.47 and 98.26%) of its crystalline nature (Fig. 6). However, in the IVS320-βCD/KN system, the reflection corresponding to IVS320 at 14.34° disappeared, the intensity of reflections at 28.22° and 24.38° was reduced, while the peak at 10.30° remained practically unvaried. As a consequence, this system showed the lowest crystallinity degree (86.06%) among the complexes prepared with βCD.

On the other hand, a more significant reduction in the crystallinity degree was detected for IVS320-MβCD systems. All diffractograms showed the disappearance of most of the crystalline reflections ascribed to IVS320. In addition, two wide halos similar to those of MβCD alone were observed, suggesting the formation of inclusion complexes [40].

Among the IVS320-MβCD systems prepared using different methods, the IVS320-MβCD/RE one stood out with a crystallinity percentage of only 24.75%, which corresponds to a 74.44% crystallinity reduction compared to IVS320. The absence of some peaks and reduction of other crystalline reflections indicated amorphization of IVS320 in these systems, suggesting its incorporation in cyclodextrin and formation of inclusion complexes, probably due to a better drug dispersion in the binary system [45]. The increase in the amorphous content of the IVS320 was verified in the following decreasing order of crystallinity degree in the systems: IVS320-MβCD/RE (24.75%) < IVS320-MβCD/KN (26.74%) < IVS320-MβCD/PM (52.09%).

3.1.5. Scanning Electron Microscopy

The SEM images of IVS320, CDs (βCD and MβCD) and IVS320-cyclodextrin systems are illustrated in Fig. 7. Pure IVS320 showed well-defined crystals of irregular size, a morphological aspect that confirms the XRD results. On the other hand, βCD and MβCD exhibited irregularly shaped and spherical particles, respectively, both of variable size [38].

The micrographs of the IVS320-βCD/PM and IVS320-βCD/KN systems revealed particles with irregular shape and different morphologies of both components, while that of the IVS320-βCD/RE system confirmed

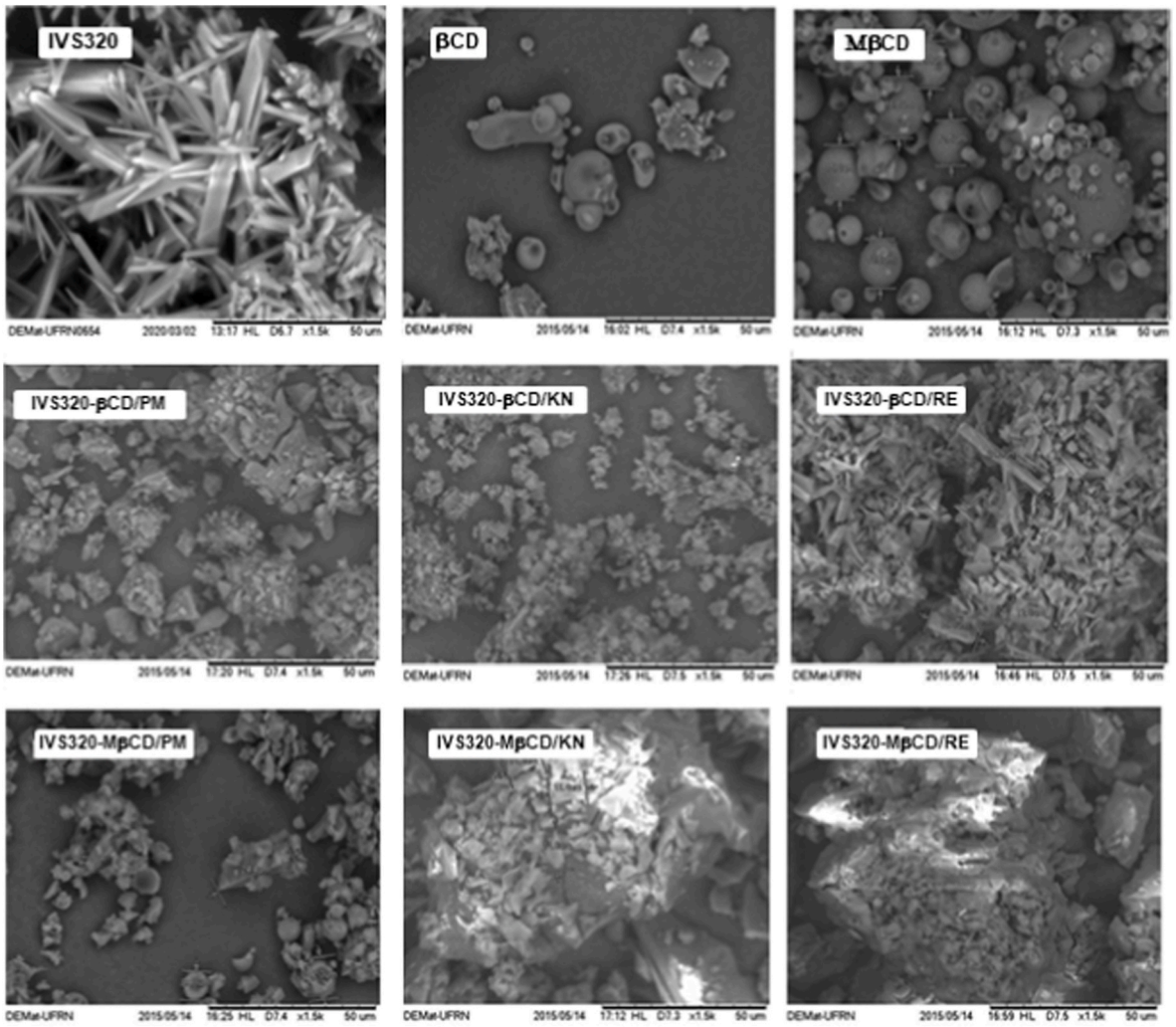

Fig. 7. Scanning electron microscopy images of single compounds: IVS320, βCD, MβCD; of inclusion complexes prepared with βCD by physical mixture (IVS320-βCD/PM), kneading (IVS320-βCD/KN), rotary evaporation (IVS320-βCD/RE); and of inclusion complexes prepared with MβCD by physical mixture (IVS320-MβCD/PM), kneading (IVS320-MβCD/KN), rotary evaporation (IVS320-MβCD/RE).

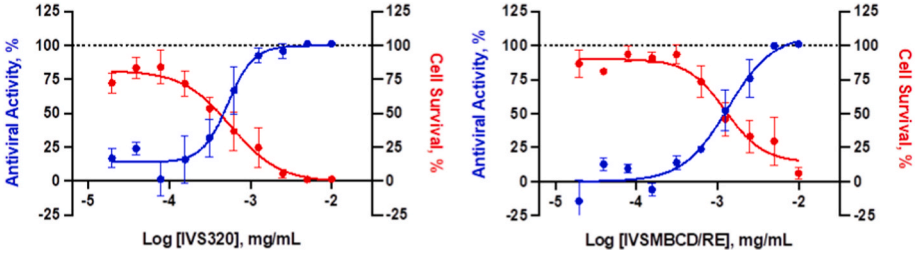

Fig. 8. *In vitro* antiviral activity (blue curves) and cytotoxic activity (red curves) of IVS320 and the IVS320-MβCD/RE complex against SARS-CoV-2. Values are expressed as mean ± standard error of the mean. (For interpretation of the references to colour in this figure legend, the reader is referred to the Web version of this article.)

the crystalline nature already evidenced by XRD for both the drug and this complex. The morphological profile of IVS320-MβCD systems was very different from that of IVS320. In fact, while in the IVS320-MβCD/PM micrograph it was possible to notice some oval shapes corresponding to MβCD, those of IVS320-MβCD/KN and IVS320-MβCD/RE did not evidence any structure similar to IVS320 crystals or to MβCD spheres. Such changes in shape and morphological aspect suggest the formation of inclusion complexes with CDs, as previously proposed [26,38].

3.2. Phenotypic assay with SARS-CoV-2

IVS320 and IVS320-MβCD/RE, which exhibited the highest reduction of crystallinity degree among complexes, were assessed for their *anti*-SARS-CoV-2 activity at different concentrations.

Both systems were able to inhibit SARS-CoV-2 infection *in vitro* with a concentration-response profile (Fig. 8), showing concentrations causing a 50% reduction of virus infection (EC_{50}) of 0.47 and 1.22 μg/mL, respectively. These values mean that the selected inclusion complex

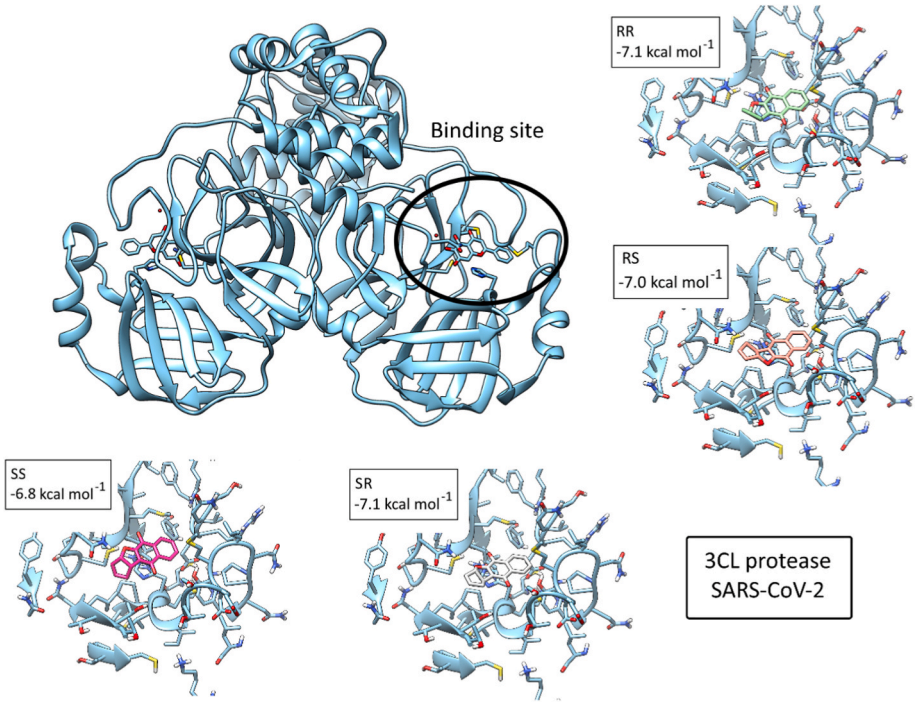

Fig. 9. Scheme of the molecular docking study performed to explain IVS320 *anti*-SARS-CoV-2 activity. $3CL^{pro}$ binding site complexed with 5,6,7-trihydroxy-2-phenyl-4H-chromen-4-one (black circle) was used to dock all possible IVS320 isomers (*RR*, *RS*, *SS*, and *SR*). Each configuration presents an Autodock Vina [37] score expressed in kcal mol^{-1}. Affinity can be measured by the score: the more negative the score, the higher the affinity.

was able to guarantee a similar inhibitory effect as pure IVS320, likely due to a synergistic effect of the drug and cyclodextrin.

3.3. SARS-CoV-2 3CL protease molecular docking simulations

A molecular docking study was conducted to check the ability of IVS320 to interact with the SARS-CoV-2 viral protein (3CL protease), an enzyme playing an essential role in the virus life cycle [46]. IVS320 owns great similarity with previously synthesized inhibitors tested against this enzyme [47], besides having a size compatibility with its catalytic site. Particularly, the binding site of 5,6,7-trihydroxy-2-phenyl-4H-chromen-4-one (PDB ChemId: 3WL), studied by X-ray crystallography (PDB Id: 6M2N), has great similarity with IVS320 as regards volume and molecular structure. Hence, we conducted molecular docking studies also to understand the mechanism of action that could explains the strong antiviral activity discussed in the previous section.

It is possible to see in Fig. 9 that the fitting of IVS320 was satisfactory with a good site occupancy. The four isomers of the drug (*RR*, *RS*, *SS*, and *SR*) had similar affinities, which suggests that the mixture of isomers would probably have the same activity as the individual compounds. These results raise the need for tests on the isolated enzyme to confirm the hypotheses put forward.

It is worth mentioning that, while the antifungal and antiparasitic potential of IVS320 has already been mentioned in the literature [17,18,41], no antiviral activity has been reported prior to this study. This emphasizes even more the importance of the antiviral potential of IVS320 and broadens the possibilities of its biological applications.

3.4. In vitro antichagasic activity

The antichagasic activities of IVS320 and IVS320-cyclodextrin systems, expressed as percent inhibition of the growth of *Trypanosoma cruzi* Y strain epimastigotes, are illustrated in Fig. 10.

The inhibition effect of IVS320 on growth was similar to that of benznidazole taken as a reference drug in the concentration range of 100 to 10 μg/mL, showing approximately 48% inhibition at the highest concentration. In general, the complexes prepared with both cyclodextrins showed, at the highest concentration, higher percent inhibitions than the drug alone, namely 48% (IVS320-βCD/PM), 70% (IVS320-βCD/KN) and 51% (IVS320-βCD/RE), and 72% (IVS320-MβCD/PM), 54% (IVS320-MβCD/KN) and 47% (IVS320-MβCD/RE), respectively.

Indeed, the systems prepared with MβCD, which showed greater reductions in the crystallinity degree than those prepared with βCD, were expected to exert a stronger antichagasic effect, especially IVS320-MβCD/RE that had the lowest crystallinity degree (24.75%). Surprisingly, however, the strongest inhibitory activities at 100 μg/mL were found with IVS320-βCD/KN (70%), whose crystallinity degree was still high (86.06%) although lower than those of the other two IVS320-βCD complexes, and with IVS320-MβCD/PM (72%), which showed, among the IVS320-MβCD complexes, the lowest reduction in crystallinity degree (52.09%).

In simpler words, the increase in antichagasic activity of IVS320 was not directly proportional to the decrease in the crystallinity degree of complexes; therefore, other factors may have played an important role. Among these, one can think of a synergistic effect of IVS320 and cyclodextrins, considering that a) βCD and MβCD exerted 19 and 51% inhibitory activities, respectively, when used alone at concentration of 100 μg/mL, b) the IVS320-βCD/KN system, contrary to IVS320, showed inhibitory activity even at the lowest concentration (2.5 μg/mL), and c) the IVS320-βCD/KN and IVS320-MβCD/PM systems exhibited stronger inhibitory effect than free IVS320 at the two highest concentrations (100 and 50 μg/mL).

These results as a whole demonstrate that the antichagasic effect of the drug was enhanced by the presence of CD in inclusion complexes.

4. Conclusions

Different IVS320-containing inclusion complexes were prepared with either β-cyclodextrin (β-CD) or methyl-β-cyclodextrin (Mβ-CD) using different methods, namely physical mixture (PM), kneading (KN) and rotary evaporation (RE). Characterization techniques showed changes in the thermal behavior, spectral properties and crystalline

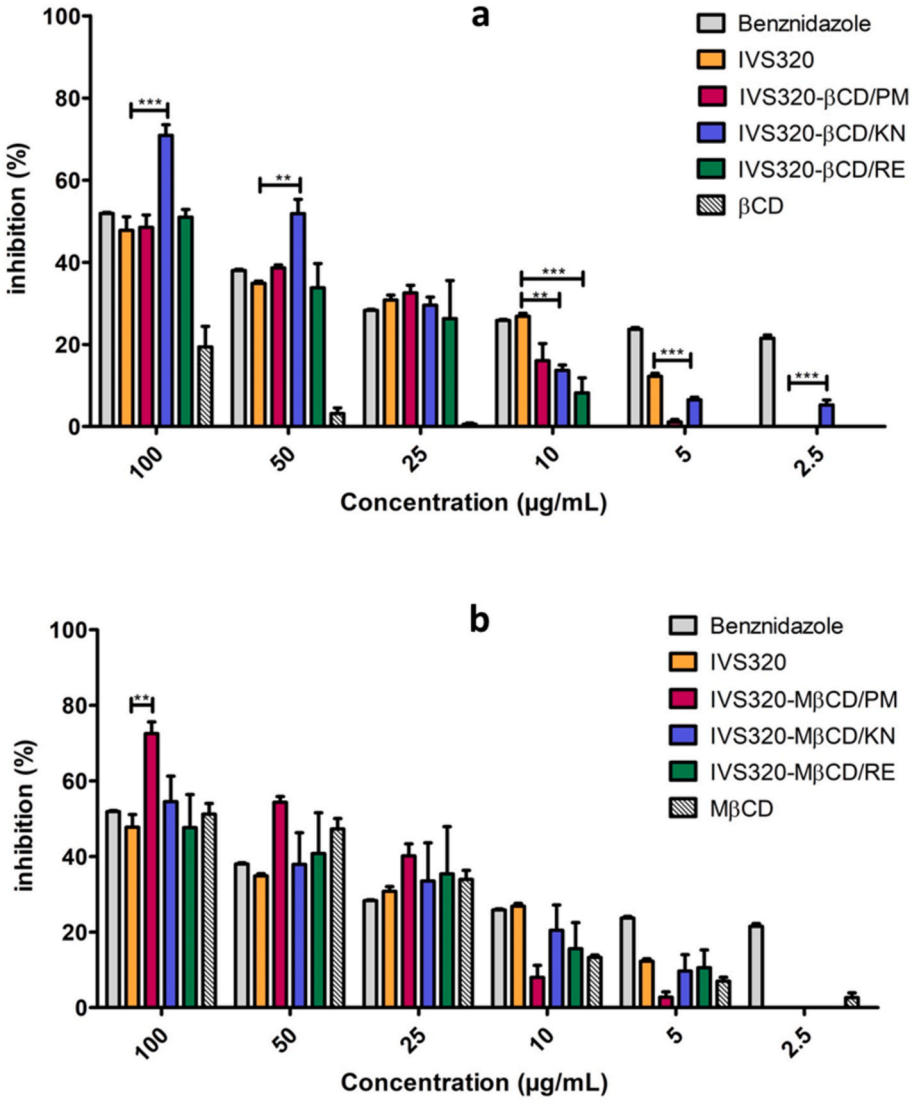

Fig. 10. *In vitro* antichagasic activity of (a) IVS320-βCD and (b) IVS320-MβCD systems against epimastigotes of *T. cruzi* Y strain after 24 h incubation. ***$p < 0.0001$ and **$p < 0.001$. ANOVA followed by Dunnett's *t*-test was used for multiple comparisons.

profiles of these systems compared to the individual constituents. Such findings suggested the formation of inclusion complexes, which led to an increase in some of the drug biological activities, probably due to the synergistic interactions between IVS320 and cyclodextrins. The antichagasic activity proved to be satisfactory, with the strongest inhibition of *Trypanosoma cruzi* epimastigote growth exerted by the IVS320-βCD/KN and IVS320-MβCD/PM systems at a concentration of 100 μg/mL. On the other hand, the highest reduction in the crystallinity degree was observed for the IVS320-MβCD/RE system. The activity of IVS320 and the IVS320-MβCD/RE system was also assessed *in vitro* against the SARS-CoV-2 virus, something that has not yet been reported so far. These preliminary results demonstrated high potential of both compounds evaluated to fight its infection, which was theoretically confirmed by docking studies showing the drug interaction with the viral 3CL protein active site.

CRediT authorship contribution statement

Verônica da Silva Oliveira: Investigation, Writing - original draft, Writing - review & editing. Cláudia Cândida Silva: Formal analysis. Johny Wysllas de Freitas Oliveira: Methodology. Marcelo de Sousa da Silva: Formal analysis. Patricia Garcia Ferreira: Methodology. Fernando de Carvalho da Siva: Methodology. Vitor Francisco Ferreira: Methodology. Euzébio Guimarães Barbosa: Formal analysis. Cecília Gomes Barbosa: Methodology. Carolina Borsoi. Moraes: Formal analysis. Lucio Holanda Gondim Freitas-Junior: Formal analysis, Resources. Attilio Converti: Writing - review & editing. Ádley Antonini Neves de Lima: Conceptualization, Writing - review & editing, Supervision, Project administration, Funding acquisition.

Declaration of competing interest

The authors declare no competing interest.

Data availability

No data was used for the research described in the article.

Acknowledgements

The authors thank the Coordination for the Improvement of Higher Education Personnel (CAPES) and the National Council for Scientific and Technological Development (CNPq) for their financial support. This study was supported by the CAPES — number 88887.505029/2020–00.

Cecilia Gomes Barbosa receives a scholarship funded by CAPES — number 88887.643352/2021–00.

References

[1] M.C.L.C. Freire, G.D. Noske, N.V. Bitencourt, P.R.S. Sanches, N.A. Santos-Filho, V. O. Gawriljuk, E.P. de Souza, V.H.R. Nogueira, M.O. de Godoy, A.M. Nakamura, R. S. Fernandes, A.S. Godoy, M.A. Juliano, B.M. Peres, C.G. Barbosa, C.B. Moraes, L.H. G. Freitas-Junior, E.M. Cilli, R.V.C. Guido, G. Oliva, Non-toxic dimeric peptides derived from the bothropstoxin-I are potent SARS-CoV-2 and papain-like protease inhibitors, Molecules 26 (2021), e04896, https://doi.org/10.3390/molecules26164896.

[2] M. Tatar, M.R. Faraji, J. Montazeri Shoorekchali, J.A. Pagán, F.A. Wilson, The role of good governance in the race for global vaccination during the COVID-19 pandemic, Sci. Rep. 11 (2021), e22440, https://doi.org/10.1038/s41598-021-01831-0.

[3] D. Aminin, S. Polonik, 1,4-Naphthoquinones: some biological properties and application, Chem. Pharm. Bull. 68 (2020) 46–57, https://doi.org/10.1248/cpb.c19-00911.

[4] D.V.C. Mendonça, G.S.V. Tavares, D.P. Lage, T.G. Soyer, L.M. Carvalho, D.S. Dias, P.A.F. Ribeiro, F.M. Ottoni, L.M.R. Antinarelli, D.L. Vale, F. Ludolf, M.C. Duarte, E. S. Coimbra, M.A. Chávez-Fumagalli, B.M. Roatt, D. Menezes-Souza, J. M. Barichello, R.J. Alves, E.A.F. Coelho, In vivo antileishmanial efficacy of a naphthoquinone derivate incorporated into a Pluronic ® F127-based polymeric micelle system against *Leishmania amazonensis* infection, Biomed. Pharmacother. 109 (2019) 779–787, https://doi.org/10.1016/j.biopha.2018.10.143.

[5] T.F. Borgati, J.D. de Souza Filho, A.B. de Oliveira, A complete and unambiguous 1H and 13C NMR signals assignment of para-naphthoquinones, ortho- and para-furanonaphthoquinones, J. Braz. Chem. Soc. 30 (2019) 1138–1149, https://doi.org/10.21577/0103-5053.20190009.

[6] M. Dong, D. Liu, Y.H. Li, X.Q. Chen, K. Luo, Y.M. Zhang, R.T. Li, Naphthoquinones from *Onosma paniculatum* with potential anti-inflammatory activity, Planta Med. 83 (2017) 631–635, https://doi.org/10.1055/s-0042-120545.

[7] G. Kapadia, G. Rao, R. Sridhar, E. Ichiishi, M. Takasaki, N. Suzuki, T. Konoshima, A. Iida, H. Tokuda, Chemoprevention of skin cancer: effect of *Lawsonia inermis* L. (Henna) leaf powder and its pigment artifact, lawsone in the Epstein- Barr virus early antigen activation assay and in two-stage mouse skin carcinogenesis models, Anti Cancer Agents Med. Chem. 13 (2013) 1500–1507, https://doi.org/10.2174/18715206113139990096.

[8] V.C. Roa-Linares, Y. Miranda-Brand, V. Tangarife-Castaño, R. Ochoa, P.A. García, M.Á. Castro, L. Betancur-Galvis, A.S. Feliciano, Anti-herpetic, anti-dengue and antineoplastic activities of simple and heterocycle-fused derivatives of terpenyl-1,4-naphthoquinone and 1,4-anthraquinone, Molecules 24 (2019), e01279, https://doi.org/10.3390/molecules24071279.

[9] S.H. Wang, C.Y. Lo, Z.H. Gwo, H.J. Lin, L.G. Chen, C.D. Kuo, J.Y. Wu, Synthesis and biological evaluation of lipophilic 1,4-naphthoquinone derivatives against human cancer cell lines, Molecules 20 (2015) 11994–12015, https://doi.org/10.3390/molecules200711994.

[10] A.O. da Silva, R.S. Lopes, R.V. de Lima, C.S.S. Tozatti, M.R. Marques, S. de Albuquerque, A. Beatriz, D.P. de Lima, Synthesis and biological activity against *Trypanosoma cruzi* of substituted 1,4-naphthoquinones, Eur. J. Med. Chem. 60 (2013) 51–56, https://doi.org/10.1016/j.ejmech.2012.11.034.

[11] L.I. López López, S.D. Nery Flores, S.Y. Silva Belmares, A. Sáenz Galindo, Naphthoquinones: biological properties and synthesis of lawsone and derivatives — a structured review, Vitae 21 (3) (2014) 248–258.

[12] J.M. Sánchez-Calvo, G.R. Barbero, G. Guerrero-Vásquez, A.G. Durán, M. Macías, M. A. Rodríguez-Iglesias, J.M.G. Molinillo, F.A. Macías, Synthesis, antibacterial and antifungal activities of naphthoquinone derivatives: a structure–activity relationship study, Med. Chem. Res. 25 (2016) 1274–1285, https://doi.org/10.1007/s00044-016-1550-x.

[13] A. Sendl, J.L. Chen, S.D. Jolad, C. Stoddart, E. Rozhon, M. Kernan, W. Nanakorn, M. Balick, Two new naphthoquinones with antiviral activity from *Rhinacanthus nasutus*, J. Nat. Prod. 59 (1996) 808–811, https://doi.org/10.1021/np9601871.

[14] S.C. Bourguignon, D.F.B. Cavalcanti, A.M.T. de Souza, H.C. Castro, C.R. Rodrigues, M.G. Albuquerque, D.O. Santos, G.G. da Silva, F.C. da Silva, V.F. Ferreira, R.T. de Pinho, C.R. Alves, *Trypanosoma cruzi*: insights into naphthoquinone effects on growth and proteinase activity, Exp. Parasitol. 127 (2011) 160–166, https://doi.org/10.1016/j.exppara.2010.07.007.

[15] C.M. Cascabulho, M. Meuser-Batista, K.C.G. de Moura, M.D.C. Pinto, T.L.A. Duque, K.C. Demarque, A.C.R. Guimarães, P.P. de A. Manso, M. Pelajo-Machado, G. M. Oliveira, S.L. De Castro, R.F.S. Menna-Barreto, Antiparasitic and anti-inflammatory activities of β-lapachone-derived naphthoimidazoles in experimental acute *Trypanosoma cruzi* infection, Mem. Inst. Oswaldo Cruz 115 (2020), e190389, https://doi.org/10.1590/0074-02760190389.

[16] A.A.D.S. Naujorks, A.O. Da Silva, R.D.S. Lopes, S. De Albuquerque, A. Beatriz, M. R. Marques, D.P. De Lima, Novel naphthoquinone derivatives and evaluation of their trypanocidal and leishmanicidal activities, Org. Biomol. Chem. 13 (2015) 428–437, https://doi.org/10.1039/c4ob01869a.

[17] C.P.V. Freire, S.B. Ferreira, N.S.M. De Oliveira, A.B.J. Matsuura, I.L. Gama, F.D. C. Da Silva, M.C.B.V. De Souza, E.S. Lima, V.F. Ferreira, Synthesis and biological evaluation of substituted α- and β-2,3-dihydrofuran naphthoquinones as potent anticandidal agents, Med. Chem. Commun. 1 (2010) 229–232, https://doi.org/10.1039/c0md00074d.

[18] E.D. Dantas, F.J.J. de Souza, W.N.L. Nogueira, C.C. Silva, P.H.A. de Azevedo, C.F. S. Aragão, P.D.O. de Almeida, M.F. do C. Cardoso, F. de C. da Silva, E.P. de Azevedo, E.G. Barbosa, E.S. Lima, V.F. Ferreira, Á.A.N. de Lima, Characterization and trypanocidal activity of a novel pyranaphthoquinone, Molecules 22 (2017), e01631, https://doi.org/10.3390/molecules22101631.

[19] P. Chaudhari, V.M. Ghate, S.A. Lewis, Supramolecular cyclodextrin complex: diversity, safety, and applications in ocular therapeutics, Exp. Eye Res. 189 (2019), e107829, https://doi.org/10.1016/j.exer.2019.107829.

[20] A.A.N. Lima, J.L. Soares-Sobrinho, J.L. Silva, R.A.C. Corrêa-Júnior, M.A.M. Lyra, F. L.A. Santos, B.G. Oliveira, M.Z. Hernandes, L.A. Rolim, P.J. Rolim-Neto, The use of solid dispersion systems in hydrophilic carriers to increase benznidazole solubility, J. Pharmacol. Sci. 100 (2011) 2443–2451, https://doi.org/10.1002/jps.

[21] V. da S. Oliveira, A.S. de Almeida, I. da S. Albuquerque, F.Í.C. Duarte, B.C.S. H. Queiroz, A. Converti, Á.A.N. de Lima, Therapeutic applications of solid dispersions for drugs and new molecules: in vitro and in vivo activities, Pharmaceutics 12 (2020), e00933, https://doi.org/10.3390/pharmaceutics12100933.

[22] E.B. Ferreira, W.F. da Silva Júnior, J.G. de Oliveira Pinheiro, A.G. da Fonseca, T.M. A. Moura Lemos, H.A. de Oliveira Rocha, E.P. de Azevedo, F.J.B. Mendonça Junior, Á.A.N. De Lima, Characterization and antiproliferative activity of a novel 2-aminothiophene derivative-β-cyclodextrin binary system, Molecules 23 (2018), e03130, https://doi.org/10.3390/molecules23123130.

[23] S. Song, K. Gao, R. Niu, J. Wang, J. Zhang, C. Gao, B. Yang, X. Liao, Inclusion complexes between chrysin and amino-appended β-cyclodextrins (ACDs): binding behavior, water solubility, in vitro antioxidant activity and cytotoxicity, Mater. Sci. Eng. C 106 (2020), e110161, https://doi.org/10.1016/j.msec.2019.110161.

[24] A.M. Rubim, J.B. Rubenick, M. Maurer, L.V. Laporta, C.M.B. Rolim, Inclusion complex of amiodarone hydrochloride with cyclodextrins: preparation, characterization and dissolution rate evaluation, Braz. J. Pharm. Sci. 53 (2017), e16083, https://doi.org/10.1590/s2175-97902017000216083.

[25] P. Jansook, N. Ogawa, T. Loftsson, Cyclodextrins: structure, physicochemical properties and pharmaceutical applications, Int. J. Pharm. 535 (2018) 272–284, https://doi.org/10.1016/j.ijpharm.2017.11.018.

[26] T.S.S. Magalhães, A. de, P.C. de O. Macedo, S.Y.K. Pacheco, S.S. da Silva, E. G. Barbosa, R.R. Pereira, R.M.R. Costa, J.O.C. Silva Junior, M.A. da Silva Ferreira, J.C. de Almeida, P.J.R. Neto, A. Converti, Á.A.N. de Lima, Development and evaluation of antimicrobial and modulatory activity of inclusion complex of euterpe oleracea mart oil and β-cyclodextrin or HP-β-cyclodextrin, Int. J. Mol. Sci. 21 (2020), e00942, https://doi.org/10.3390/ijms21030942.

[27] P. Tang, S. Li, L. Wang, H. Yang, J. Yan, H. Li, Inclusion complexes of chlorzoxazone with β- and hydroxypropyl-β-cyclodextrin: characterization, dissolution, and cytotoxicity, Carbohydr. Polym. 131 (2015) 297–305, https://doi.org/10.1016/j.carbpol.2015.05.055.

[28] B. Gürten, E. Yenigül, A.D. Sezer, S. Malta, Complexation and enhancement of temozolomide solubility with cyclodextrins, Braz. J. Pharm. Sci. 54 (2018), e17513, https://doi.org/10.1590/s2175-97902018000217513.

[29] M.D. Vukic, N.L. Vukovic, S.L. Popovic, D.V. Todorovic, P.M. Djurdjevic, S. D. Matic, M.M. Mitrovic, A.M. Popovic, M.M. Kacaniova, D.D. Baskic, Effect of β-cyclodextrin encapsulation on cytotoxic activity of acetylshikonin against HCT-116 and MDA-MB-231 cancer cell lines, Saudi Pharmaceut. J. 28 (2020) 136–146, https://doi.org/10.1016/j.jsps.2019.11.015.

[30] P. Mahalapbutr, P. Wonganan, T. Charoenwongpaiboon, M. Prousoontorn, W. Chavasiri, T. Rungrotmongkol, Enhanced solubility and anticancer potential of mansonone G by β-cyclodextrin-based host-guest complexation: a computational and experimental study, Biomolecules 9 (2019), e00545, https://doi.org/10.3390/biom9100545.

[31] DXTA, Version 2.6. [S. l.]: Shimadzu, 1995, 1 CD.

[32] Sales-Medina, D.F., Ferreira, L.R.P., Romera, L.M.D., Golcalves, K.R., Guido, R.V. C., Courtemanche, G., Buckeridge, M.S., Durigon, E.L., Moraes, C.B., Freitas-Junior, L.H., 2020. Discovery of clinically approved drugs capable of inhibiting SARS-CoV-2. BioRxiv 2020.07.09, e196337. https://doi.org/https://doi.org/10.1101/2020.07.09.196337.

[33] M.D. Hanwell, D.E. Curtis, D.C. Lonie, T. Vandermeerschd, E. Zurek, G. R. Hutchison, Avogadro: an advanced semantic chemical editor, visualization, and analysis platform, J. Cheminf. 4 (2012), e00017, https://doi.org/10.1186/1758-2946-4-17.

[34] J.J.P. Stewart, Optimization of parameters for semiempirical methods VI: more modifications to the NDDO approximations and re-optimization of parameters, J. Mol. Model. 19 (2013) 1–32, https://doi.org/10.1007/s00894-012-1667-x.

[35] E.F. Pettersen, T.D. Goddard, C.C. Huang, G.S. Couch, D.M. Greenblatt, E.C. Meng, T.E. Ferrin, UCSF Chimera - a visualization system for exploratory research and analysis, J. Comput. Chem. 25 (2004) 1605–1612, https://doi.org/10.1002/jcc.20084.

[36] H. xia Su, S. Yao, W. feng Zhao, M. jun Li, J. Liu, W. juan Shang, H. Xie, C. qiang Ke, H. chen Hu, M. na Gao, K. qian Yu, H. Liu, J. shan Shen, W. Tang, L. ke Zhang, G. fu Xiao, L. Ni, D. wen Wang, J. ping Zuo, H. liang Jiang, F. Bai, Y. Wu, Y. Ye, Y. chun Xu, Anti-SARS-CoV-2 activities in vitro of Shuanghuanglian preparations and bioactive ingredients, Acta Pharmacol. Sin. 41 (2020) 1167–1177, https://doi.org/10.1038/s41401-020-0483-6.

[37] O. Trott, A.J. Olson, AutoDock Vina: improving the speed and accuracy of docking with a new scoring function, efficient optimization, and multithreading, J. Comput. Chem. 31 (2010) 455–461, https://doi.org/10.1002/jcc.21334.

[38] P.S. Santos, L.K.M. Souza, T.S.L. Araujo, J.V.R. Medeiros, S.C.C. Nunes, R. A. Carvalho, A.C.C. Pais, F.J.B. Veiga, L.C.C. Nunes, A. Figueiras, Methyl-β-cyclodextrin inclusion complex with β-caryophyllene: preparation, characterization, and improvement of pharmacological activities, ACS Omega 2 (2017) 9080–9094, https://doi.org/10.1021/acsomega.7b01438.

[39] M. Banchero, S. Ronchetti, L. Manna, Characterization of ketoprofen/methyl-β-cyclodextrin complexes prepared using supercritical carbon dioxide, J. Chem. 2013 (2013), e583952, https://doi.org/10.1155/2013/583952.
[40] S.R.S. Rudrangi, V. Trivedi, J.C. Mitchell, S.R. Wicks, B.D. Alexander, Preparation of olanzapine and methyl-β-cyclodextrin complexes using a single-step, organic solvent-free supercritical fluid process: an approach to enhance the solubility and dissolution properties, Int. J. Pharm. 494 (2015) 408–416, https://doi.org/10.1016/j.ijpharm.2015.08.062.
[41] V. da S. Oliveira, E.D. Dantas, A.T. de S. Queiroz, J.W. de F. Oliveira, M. de S. da Silva, P.G. Ferreira, F. de C. da Siva, V.F. Ferreira, Á.A.N. de Lima, Novel solid dispersions of naphthoquinone using different polymers for improvement of antichagasic activity, Pharmaceutics 12 (2020), e01136, https://doi.org/10.3390/pharmaceutics12121136.
[42] N. Li, Yun Hui Zhang, Y.N. Wu, X.L. Xiong, Ya Hui Zhang, Inclusion complex of trimethoprim with β-cyclodextrin, J. Pharm. Biomed. Anal. 39 (2005) 824–829, https://doi.org/10.1016/j.jpba.2005.05.011.
[43] T. Suzuki, A. Ei, Y. Takada, H. Uehara, T. Yamanobe, K. Takahashi, Modification of physical properties of poly(L-lactic acid) by addition of methyl-β-cyclodextrin, Beilstein J. Org. Chem. 10 (2014) 2997–3006, https://doi.org/10.3762/bjoc.10.318.
[44] M.D. Veiga, M. Merino, D. Fernández, R. Lozano, Characterization of some cyclodextrin derivatives by thermal analysis, J. Therm. Anal. Calorim. 68 (2002) 511–516, https://doi.org/10.1023/A:1016091803317.
[45] A.C.S.G.V. Santana, D. Nadvorny, T.D. da Rocha Passos, M.F. de La Roca Soares, J. L. Soares-Sobrinho, Influence of cyclodextrin on posaconazole stability, release and activity: improve the utility of the drug, J. Drug Deliv. Sci. Technol. 53 (2019), e101153, https://doi.org/10.1016/j.jddst.2019.101153.
[46] T. Pillaiyar, M. Manickam, V. Namasivayam, Y. Hayashi, S.H. Jung, An overview of severe acute respiratory syndrome-coronavirus (SARS-CoV) 3CL protease inhibitors: peptidomimetics and small molecule chemotherapy, J. Med. Chem. 59 (2016) 6595–6628, https://doi.org/10.1021/acs.jmedchem.5b01461.
[47] S. Koulgi, V. Jani, M. Uppuladinne, U. Sonavane, A.K. Nath, H. Darbari, R. Joshi, Drug repurposing studies targeting SARS-CoV-2: an ensemble docking approach on drug target 3C-like protease (3CLpro), J. Biomol. Struct. Dyn. 39 (2021) 5735–5755, https://doi.org/10.1080/07391102.2020.1792344.